Mineralogical Magazine (2019), **83**, 695–703
doi:10.1180/mgm.2019.31

CAMBRIDGE UNIVERSITY PRESS

Article

Ognitite, NiBiTe, a new mineral species, and Co-rich maucherite from the Ognit ultramafic complex, Eastern Sayans, Russia

Andrei Y. Barkov[1]*, Luca Bindi[2], Nobumichi Tamura[3], Gennadiy I. Shvedov[4], Björn Winkler[5], Camelia V. Stan[3], Wolfgang Morgenroth[5], Robert F. Martin[6], Federica Zaccarini[7] and Christopher J. Stanley[8]

[1]Research Laboratory of Industrial and Ore Mineralogy, Cherepovets State University, 5 Lunacharsky Avenue, 162600 Cherepovets, Russia; [2]Dipartimento di Scienze della Terra, Università degli Studi di Firenze, Via G. La Pira 4, I-50121 – Firenze, Italy; [3]Advanced Light Source, 1 Cyclotron Road, Lawrence Berkeley National Laboratory, Berkeley, CA 94720-8229, USA; [4]Institute of Mining, Geology and Geotechnology, Siberian Federal University, 95 Avenue Prospekt im. gazety "Krasnoyarskiy Rabochiy", 660025 Krasnoyarsk, Russia; [5]Inst. f. Geowissenschaften, Universität Frankfurt, Altenhöferallee 1, DE-60438 Frankfurt a. M., Germany; [6]Department of Earth and Planetary Sciences, McGill University, 3450 University Street, Montreal, Quebec H3A 0E8, Canada; [7]University of Leoben, Department of Applied Geosciences and Geophysics, Peter Tunner Strasse 5, A-8700 Leoben, Austria; and [8]Economic and Environmental Earth Sciences Division, The Natural History Museum, Cromwell Road, London SW7 5BD, United Kingdom

Abstract

We describe the new species ognitite, NiBiTe, and a Co-rich variety of maucherite, hitherto unreported; both were discovered in the Ognit ultramafic complex of Neoproterozoic age in Eastern Sayans, Russia. The mean composition of ognitite ($n = 7$) is: Ni 17.05, Fe 0.07, Cu 0.14, Pd 0.14, Te 32.53, Bi 49.64, total 99.57 wt.%, corresponding to: $(Ni_{1.11}Cu_{0.008}Fe_{0.005}Pd_{0.005})_{\Sigma 1.13}Bi_{0.90}Te_{0.97}$ (Σ atoms = 3 apfu). Ognitite is trigonal, space group $P3m1$ [$R_1 = 0.0276$ for 81 reflections with $F_o > 4\sigma(F_o)$]. The unit-cell parameters derived from the single-crystal X-ray diffraction data are: $a = 3.928(1)$ Å, $c = 5.385(1)$ Å and $V = 71.95(4)$ Å^3, with Z = 1. The c:a ratio is 1.37. The powder X-ray diffraction data obtained on the same fragment used for the single-crystal study are: $a = 3.9332(4)$ Å, $c = 5.3920(6)$ Å and $V = 72.24(1)$ Å^3. Ognitite exhibits the brucite-type structure with edge-sharing $NiTe_3Bi_3$ octahedra forming sheets parallel to (0001). It is related to melonite, but is distinct compositionally by the extreme Bi-enrichment (melonite and its synthetic analogue contain <0.4 Bi apfu), and structurally as Bi and Te are ordered at two distinct sites, leading to the loss of the centre of symmetry in ognitite.

At more than 9 wt.% Co, or ~2 apfu Co, the core of Co-rich maucherite $[(Ni,Co)_{11}As_8]$ in a zoned crystal, which is surrounded by Co-depleted orcelite, far surpasses the norm (≤1 and up to 3.9 wt.% Co). The unit-cell parameters of the Co-rich maucherite are: $a = 6.85(2)$ and $c = 21.83(5)$ Å, which are based on results of synchrotron micro-Laue diffraction.

The host rock consists of serpentine, clinochlore (Mg# 95–97) and skeletal chromite. We favour the metastable crystallisation of fluid-saturated globules of a sulfide–arsenide melt to explain the anomalous compositions of ore minerals at Ognit. These anomalies seem consistent with rapid cooling in a fluid-enriched system, possibly related to late-stage degassing of the magma, as reflected in a prominent metasomatic aureole at the contact with the enclosing gneissic rocks.

Keywords: ognitite, NiBiTe, new mineral species, Co-rich maucherite, zonation in arsenides, rapid cooling, Ognit complex, nickel-cobalt mineralisation, ultramafic rocks, Eastern Sayans, Russia

(Received 14 June 2018; accepted 11 April 2019; Accepted Manuscript online: 8 May 2019; Associate Editor: Irina O Galuskina)

Introduction

We document the occurrences and properties of two minerals of nickel, i.e. ognitite and Co-rich maucherite, discovered in the Ognit ultramafic complex, in Eastern Sayans, Russia. Ognitite has been approved as a valid species (IMA2018-006a, Barkov *et al.* 2019) by the Commission on New Minerals, Nomenclature and Classification (CNMNC) of the International Mineralogical Association (IMA). The name ognitite (Cyrillic: огнитит) is after the Ognit complex, in which the new mineral occurs. The catalogue number of the ognitite single crystal is 3292/I at the Museo di Storia Naturale of the University of Firenze, Italy.

Ognitite ($Ni_{1.1}Bi_{0.9}Te$) has a distinctly Bi-rich composition; in addition, it differs structurally from melonite. With an ideal composition $NiTe_2$, melonite generally contains no more than 0.25 atoms of Bi per formula unit (apfu), and exceptionally up to 0.4 apfu in complex solid solutions that also involve Pt and Pd (Barkov *et al.*, 2017*a*, and references therein). Such an enrichment reflects the incorporation of substantial levels of the merenskyite ($PdTe_2$) and moncheite ($PtTe_2$) components (e.g. Garuti and Rinaldi, 1986). However, ognitite shows a striking Bi enrichment without those two components.

The Co-rich maucherite represents a novel variety, unusual and hitherto unreported. Maucherite, ideally $Ni_{11}As_8$, is one of the principal carriers of Pd in various Ni–Cu–PGE (platinum-group element) deposits. We report a major enrichment of cobalt in the core of a zoned grain. At more than 9 wt.% Co, or roughly 2 apfu Co,

***Author for correspondence:** Andrei Y. Barkov, Email: ore-minerals@mail.ru
Cite this article: Barkov A.Y., Bindi L., Tamura N., Shvedov G.I., Winkler B., Stan C.V., Morgenroth W., Martin R.F., Zaccarini F. and Stanley C.J. (2019) Ognitite, NiBiTe, a new mineral species, and Co-rich maucherite from the Ognit ultramafic complex, Eastern Sayans, Russia. *Mineralogical Magazine* **83**, 695–703. https://doi.org/10.1180/mgm.2019.31

this composition far surpasses what is normally encountered: ≤1.2 wt.% Co (e.g. Fleet, 1973*a*; Wagner and Lorenz, 2002; Makovicky and Merlino, 2009) and, occasionally, up to 3.1–3.9 wt.% Co (Petruk *et al.*, 1971; Gritsenko and Spiridonov, 2008; Raič *et al.*, 2015).

We seek to establish the circumstances that could have led to the mineralogical anomalies observed. In addition, we describe a characteristic zonation, hitherto unreported, in Ni–(Co) arsenides at Ognit. Our findings extend the knowledge of the pattern of behaviour and extent of solid solution, and provide a useful insight into the ore-forming environments leading to Cu–Ni–PGE mineralisation in ultramafic complexes.

Background information

As noted, melonite and its synthetic analogue normally contain <0.4 apfu Bi (Barkov *et al.*, 2017*a*, and references therein). Maucherite generally contains between 18 and 265 ppm Pd (Gervilla *et al.*, 2000). In experiments, the extent of Pd-enrichment increases with decreasing temperature, to attain 5.5 at.% Pd at 450°C (Gervilla *et al.*, 1994). Elevated contents, up to 1.5–1.8 wt.% Pd, are known in grains of maucherite from the Sudbury, Canada and Noril'sk, Russia complexes (Cabri and Laflamme, 1976; Gritsenko and Spiridonov, 2008). In addition, maucherite is one of the principal arsenides deposited from melts rich in As under experimental and natural conditions (Prichard *et al.*, 2013). Arsenic-rich melts segregated experimentally *via* immiscibility from sulfide melts are capable of efficiently scavenging the initially dissolved PGE, especially Pd (Fleet *et al.*, 1993; Makovicky *et al.*, 1992). Elevated contents of Cu (and S), up to ~5 wt.% each, were documented in grains of maucherite from metamorphosed Cu–Ni ores of the Noril'sk complex, Russia (Gritsenko and Spiridonov, 2008).

Geological setting and ore-mineral associations

Both ognitite and Co-rich maucherite occur in dunite in zones of disseminated Cu–Ni–PGE sulfide mineralisation in the Ognit (or Medek) dunite–wehrlite complex of Neoproterozoic age, located at the southern margin of the Siberian Craton, Irkutskaya (Irkutsk) oblast, Russia (Figs 1*a*, *b*). The Ognit complex belongs to a suite of dunite–peridotite–pyroxenite complexes, namely Shumikha, Kingash, Golumbei, Tartai, Ognit, Zhelos, Tokty-Oi and Malyi Zadoi, associated with the Yoko–Dovyren complex in the Baikal–Patom zone. These complexes formed in a continental margin setting in the East Siberian metallogenic province (e.g. Mekhonoshin *et al.*, 2013; Tolstykh *et al.*, 2014). They give a radiometric age in the range 731–710 Ma, which is close to the range reported for the Franklin Province in northwestern Canada, 725–710 Ma, and is thus consistent with the inferred breakup of Rodinia in Neoproterozoic time (Gladkochub *et al.*, 2006; Ernst *et al.*, 2012; Tolstykh *et al.*, 2014).

The Ognit complex is a relatively small ultramafic body ≤1.5 km long at the contact of granodiorite and gneiss. It is mostly composed of dunite, wehrlite, and olivine pyroxenite. The core-like zone is essentially dunitic; elements of large-scale layering are recognised in the complex (Fig. 1*b*). A notable feature is the development of a pronounced zone of metasomatic alteration, especially at the southeastern contact.

The ultramafic rocks of the Ognit complex are variably serpentinised; they are composed of a serpentine-group mineral, clinochlore and calcic amphiboles (actinolite and tschermakite). Chromite, including skeletal grains of low-Al compositions

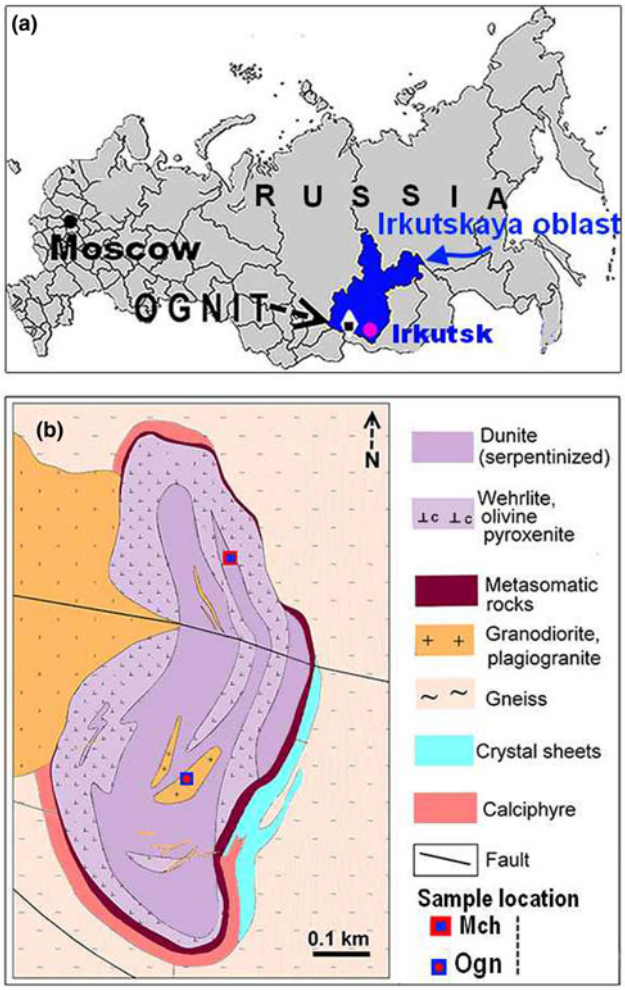

Fig. 1. (*a*) The location of the Ognit complex in the Russian Federation and (*b*) geological map of the Ognit complex, Eastern Sayans, Russia, based on various sources (Mekhonoshin *et al.*, 2013, 2018, and references therein; Oleshkevich *et al.*, pers. comm.). The sample location is shown for ognitite (labelled Ogn) and Co-rich maucherite (Mch).

(Figs 2*a*, 3, Table 1), and magnetite are common accessories. The ore zones consist of sulfides (≤3 modal%), mainly pentlandite and chalcopyrite, subordinate troilite and cubanite, rare heazlewoodite, pyrite, bornite, mackinawite, secondary chalcocite, covellite, violarite, valleriite and, occasionally, sphalerite and molybdenite. Less common/rare species of ore minerals include orcelite, maucherite, cobaltite–gersdorffite, altaite, hessite, Se-bearing galena, shandite, parkerite, native silver and Ag–Au alloy (Ag-dominant), auricupride, awaruite, native copper, graphite and native bismuth (Shvedov and Barkov, 2017).

Two associations of platinum-group minerals (PGM) exist in the Ni–Cu–PGE zones at Ognit. The first includes species rich in Ir–Ru–Os: Ru–Os disulfides (laurite–erlichmanite series), Ru–Os diarsenides (anduoite–omeiite) and sulfarsenides (platarsite–osarsite–ruarsite). These PGM, crystallising relatively early, exhibit a close affinity to primary grains of base-metal sulfides. The second association is late, more diverse, and mainly consists of Pd-rich PGM: palladium bismuthotellurides and antimonides, such as phases of the type $Pd(Bi,Te,Sb)_{1+x}$, merenskyite, michenerite, mertieite-II and stibiopalladinite, naldrettite, polarite, urvantsevite, froodite, palladogermanide (Pd_2Ge: cf. IMA2016-086) and unnamed $Pd_{2+x}Cu_{1-x}(Sb,Sn)$ (Shvedov and Barkov, 2017).

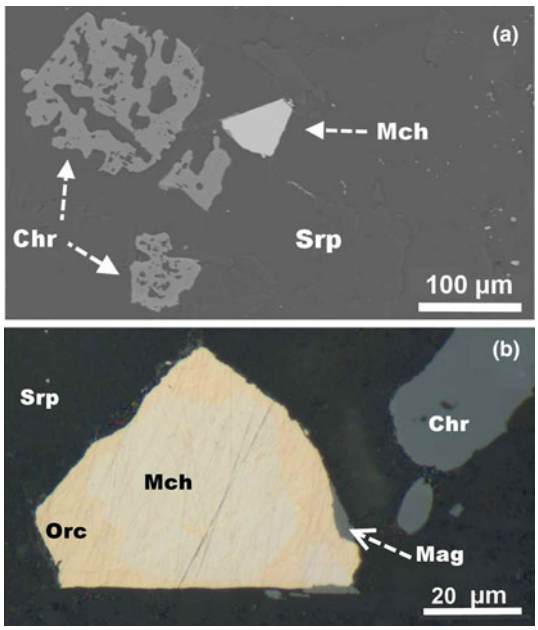

Fig. 2. A back-scattered electron (BSE) image (*a*) and reflected light microphotograph (*b*) showing the zoned grain of maucherite (Mch)–orcelite (Orc), associated with skeletal grains of chromite (Chr), hosted by fine intergrowths of serpentine (Srp) and clinochlore; Mag is secondary magnetite.

Analytical methods

Compositions of ognitite were established *via* wavelength-dispersive spectrometry (WDS) using a JEOL JXA-8900L electron microprobe, at 20 kV, 50 nA, and with a 5-μm beam size at McGill University, Montreal, Canada. The following lines and standards were used: *K*α and CoNiAs (for Ni), *K*α and metallic iron (Fe), *K*α and $CuFeS_2$ (Cu), *K*α and CoNiAs (Co), *L*α and Pd_3HgTe_3 or metallic Pd (Pd), *M*β and metallic Pt (Pt), *L*α and PbTe (Te), *M*α and Bi_2Te_3 (Bi), *M*α and PbTe (Pb), *K*α and Bi_2S_3 (S), *L*β and CoNiAs (As), and *L*β and pure Sb (Sb). The PRZ correction was applied. The counting times were 150 s for As, 60 s for Pd, Pt, Co, Sb and Pb, and 20 s for Ni, Fe, Cu, Te, Bi and S. Minimum detection limits (wt.%) are: 0.01 (S and Co), 0.02 (Fe), 0.03 (Ni), 0.04 (Cu, Pd, Pt, Pb and As), 0.05 (Sb), 0.06 (Te) and 0.08 (Bi).

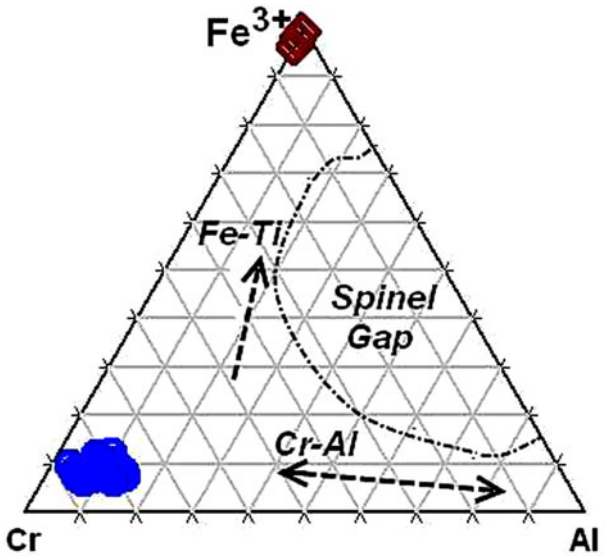

Fig. 3. Compositions of skeletal grains of chromite and associated magnetite zones (shown by blue and brown symbols, respectively) from the Ognit complex in terms of the Cr–Fe^{3+}–Al plot (atomic %). The positions of Fe–Ti and Cr–Al trends and the miscibility gap are from Barnes and Roeder (2001).

The Co-rich maucherite and associated minerals (chromite, clinochlore and serpentine) were analysed with a JEOL JXA-8200 microprobe at the E.F. Stumpfl laboratory, University of Leoben, Austria. The analytical conditions (WDS with a ≤2 μm beam) used for the zoned maucherite grain were: 20 kV, 10 nA, and 20 s counting times for the peak and 10 s for the backgrounds. The following lines and standards were used: Ni*K*α (pentlandite), Fe*K*α, S*K*α (pyrite), As*L*α, Co*K*α (skutterudite), Bi*M*α, Te*L*α (synthetic Bi_2Te_3), and Sb*L*α and Sb*L*β (Sb_2Te_3). The detection limits expressed in ppm are: 100 for As and S, 150 for Ni, Fe and 600 for Co, Sb, Bi and Te. Levels of Sb, Bi and Te were below the detection limit.

Scanning-electron microscopy (SEM) and energy-dispersive analysis (EDS) were also employed, using a MIRA 3 LMU (Tescan Ltd.) system combined with INCA Energy 450+ XMax 80 (Oxford Instruments Ltd), at the Institute of Geology and Mineralogy, Novosibirsk, Russia. The reflectance measurements on ognitite were carried out using a WTiC standard at the Natural History Museum, London, UK.

Single-crystal X-ray diffraction data were collected on the ognitite specimen using an Oxford Diffraction Xcalibur diffractometer equipped with an Oxford Diffraction CCD detector, with graphite-monochromatised Mo*K*α radiation (λ = 0.71073 Å).

The powder X-ray diffraction data were obtained on the same fragment of the ognitite grain used for the single-crystal study with an Oxford Diffraction Xcalibur PX Ultra diffractometer fitted with a 165 mm diagonal Onyx CCD detector and using copper radiation [Cu*K*α (λ = 1.54184 Å)]. The working conditions were 40 kV and 40 nA with 3 hr of exposure; the detector-to-sample distance was 7 cm. The program *CrysAlis RED* (Oxford Diffraction, 2006) was used to convert the observed diffraction rings to a conventional powder-diffraction pattern. The least-squares refinement gave the unit-cell values listed below.

We also provide results of synchrotron X-ray Laue microdiffraction measurements at beam line 12.3.2 of the Advanced Light Source (ALS), Berkeley, California, USA. A polychromatic X-ray beam (5–24 keV) was focused to approximately 2 μm × 2 μm (full width at half maximum) with Kirkpatrick–Baez mirrors. Laue diffraction patterns were collected with a PILATUS 1M area detector in reflection geometry, with the sample inclined 45° to the primary beam, and the area detector was set to 90°. The Laue diffraction patterns were collected with raster scanning across the entire sample area. The patterns were indexed and analysed using *XMAS v.6* (Tamura, 2014). An energy scan (10–20 keV, 10 eV step size) was performed on single reflections to determine the lattice parameters.

Occurrence, physical and optical properties, and composition of ognitite

Ognitite forms a single homogeneous grain (80 μm × 30–40 μm) hosted by chalcopyrite; it is anhedral, irregularly shaped, and occurs next to a small grain of native bismuth (Fig. 4). The new species is metallic and opaque; its colour and streak are metallic black (powder). The value of its density (calculated) is 8.75 g/cm^3.

Table 1. Compositions of skeletal grains of chromite from the Ognit complex, Eastern Sayans.

#	1	2	3	4	5	6	7	8	9	10(R)
Wt.%										
TiO_2	0.7	1.41	0.98	1.01	0.86	0.81	1.15	1.16	1.15	0.28
Al_2O_3	3.4	4.7	3.97	5.42	5.08	3.76	6.47	5.19	5.91	0.03
Cr_2O_3	59.58	55.33	56.53	55.47	55.32	57.81	55.07	55.91	56.33	0.41
V_2O_3	0.19	0.2	0.27	0.22	0.2	0.17	0.27	0.16	0.15	0.04
FeOtot*	31.63	33.7	32.85	32.84	32.9	32.71	31.42	32.27	31.22	92.23
FeO*	26.96	27.54	26.95	26.43	25.97	27.07	26.18	27.18	26.64	29.74
Fe_2O_3*	5.19	6.84	6.55	7.11	7.7	6.27	5.83	5.65	5.09	69.44
MnO	0.99	0.89	0.95	0.94	0.89	0.94	0.88	0.92	0.89	0.06
MgO	3.27	3.53	3.32	4.05	4.1	3.24	4.35	3.37	3.99	1.06
NiO	–	0.04	0.01	0.01	–	–	0.04	0.02	0.08	0.3
ZnO	0.51	0.46	0.61	0.62	0.74	0.62	0.62	0.74	0.54	–
Total	100.77	100.95	100.15	101.3	100.86	100.69	100.86	100.29	100.77	101.36
Apfu on the basis of four oxygen atoms										
Ti	0.019	0.037	0.026	0.027	0.023	0.022	0.03	0.031	0.03	0.008
Al	0.14	0.2	0.17	0.22	0.21	0.16	0.27	0.22	0.24	0
Cr	1.68	1.54	1.6	1.53	1.54	1.63	1.51	1.57	1.56	0.01
V	0.005	0.006	0.008	0.006	0.006	0.005	0.007	0.005	0.004	0.001
Fe^{3+}	0.14	0.18	0.18	0.19	0.2	0.17	0.15	0.15	0.13	1.97
Fe^{2+}	0.8	0.81	0.8	0.77	0.76	0.81	0.76	0.81	0.78	0.94
Mn	0.03	0.027	0.029	0.028	0.027	0.028	0.026	0.028	0.026	0.002
Mg	0.17	0.19	0.18	0.21	0.21	0.17	0.23	0.18	0.21	0.06
Ni	–	0.001	0	0	–	–	0.001	0.001	0.002	0.009
Zn	0.013	0.012	0.016	0.016	0.019	0.016	0.016	0.019	0.014	–
Mg#	17	17.9	17.2	20.5	21	16.8	21.9	17.3	20.3	6
Cr#	92.2	88.8	90.5	87.3	88	91.2	85.1	87.8	86.5	91.1
Fe^{3+}#	7.1	9.5	9.1	9.6	10.4	8.6	7.9	7.8	6.9	99.3

Notes: 10(R) refers to a rim zone of skeletal grain of chromite; *FeO(tot): all Fe is expressed as FeO. FeO and Fe_2O_3 are calculated on the basis of stoichiometry and charge balance. Mg# is 100Mg/(Mg + Fe^{2+}+Mn); Cr# is 100Cr/(Cr + Al), and Fe^{3+}# is 100Fe^{3+}/(Fe^{3+} +Cr + Al).
'–' = below the detection limit

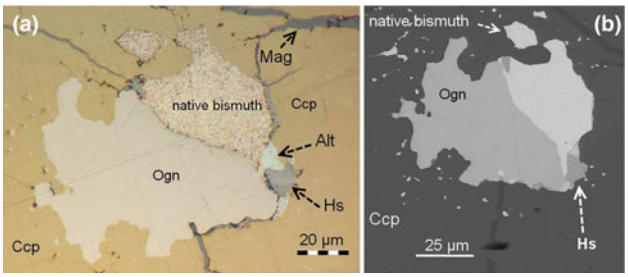

Fig. 4. Reflected light microphotograph (*a*) showing the ognitite grain (Ogn), which is hosted by chalcopyrite (Ccp), and is associated with native bismuth, hessite (Hs), altaite (Alt), and also with late veinlets of magnetite (Mag). (*b*) BSE image showing ognitite (Ogn) and associated grains, complementary to those shown in the optical photograph in (*a*). Type specimen (#3292/I).

Table 2. Reflectance values for ognitite.

λ (nm)	R_{max} (%)	R_{min} (%)	λ (nm)	R_{max} (%)	R_{min} (%)
400	52.0	51.0	560	55.5	55.1
420	52.2	51.3	580	56.3	56.0
440	52.5	51.6	**589**	**56.7**	**56.4**
460	53.0	52.1	600	57.0	56.8
470	**53.2**	**52.4**	620	57.7	57.5
480	53.4	52.6	640	58.5	58.3
500	53.9	53.2	**650**	**58.9**	**58.7**
520	54.4	53.8	660	59.2	59.0
540	54.9	54.4	680	60.0	59.8
546	**55.1**	**54.6**	700	60.8	60.6

Notes: These values were measured in air; the standard used is WTiC.
The values required by the Commission on Ore Mineralogy are given in bold.

Under reflected light, ognitite is creamy white. It is slightly to distinctly bireflectant, with a pleochroism from creamy white to slightly lighter creamy white. Ognitite is slightly to distinctly anisotropic. Internal reflections were not observed. Reflectance values of ognitite (WTiC standard, in air) are listed in Table 2.

Representative compositions of ognitite are given in Table 3. Other elements (Co, Pt, Sb, Pb, As and S) were also sought, but not detected. The mean composition (and ranges for seven point analyses, $n = 7$) are: Ni 17.05 (16.91–17.15), Fe 0.07 (0.02–0.16), Cu 0.14 (0.08–0.26), Pd 0.14 (0.09–0.16), Te 32.53 (31.79–33.67), Bi 49.64 (48.27–50.31), total 99.57 (99.01–100.07) wt.%. Minor Pd is thus present. Results of two independent methods of microprobe analyses (WDS and SEM/EDS) are in excellent agreement; they yield essentially the same empirical formula: $(Ni_{1.11}Cu_{0.008}Fe_{0.005}Pd_{0.005})_{\Sigma 1.13}Bi_{0.90}Te_{0.97}$, calculated on the basis of a total of 3 apfu. A minor extent of Ni-for-Bi substitution is thus implied. Examples of Ni–Bi substitution are known in some compounds: $LaNi_{4.7-x}Bi_xAl_{0.3}$ with $x = 0.1$, 0.2 or 0.3 (Yilmaz *et al.*, 2012) and $Bi_{2-x}Ni_xSr_2CaCu_2O_y$ with $x = 0$, 0.05, 0.1 or 0.2 (Özkurt, 2012). In addition, a mean electron number <83 at the Bi site of ognitite is consistent with the inferred presence of a lighter element (presumably Ni) at the 1*b* position. The ideal formula of ognitite is NiBiTe, which requires Ni 14.85, Bi 52.87 and Te 32.28, for a total of 100 wt.%.

An initial study of the ognitite grain was undertaken using synchrotron micro-Laue diffraction followed by a monochromator energy scan, results of which indicate that is a single phase, apparently untwinned, with $a = 3.925(5)$ Å and $c = 5.381(7)$ Å. These patterns were indexed and analysed using *XMAS v.6* (Tamura, 2014).

Ognitite is trigonal; its space group is *P*3*m*1. The unit-cell parameters derived from the single-crystal X-ray diffraction data

Table 3. Compositions of ognitite from the Ognit complex.

#	1	2	3	4	5	6	7	8	9
Ni	17.03	16.91	17.07	17.06	17.00	17.15	17.15	17.05	17.17
Pd	0.09	0.15	0.14	0.14	0.16	0.11	0.16	0.14	0
Fe	0.05	0.05	0.03	0.02	0.08	0.16	0.12	0.07	0
Cu	0.12	0.13	0.09	0.08	0.14	0.26	0.19	0.14	0
Bi	48.27	49.68	49.92	49.68	50.31	49.95	49.64	49.64	49.68
Te	33.67	32.10	32.35	32.77	31.79	32.44	32.59	32.53	33.16
Total	99.23	99.01	99.60	99.75	99.48	100.07	99.85	99.57	100.01
Compositions on the basis of 3 apfu									
Ni	1.10	1.11	1.11	1.11	1.11	1.10	1.11	1.11	1.11
Pd	0.003	0.005	0.005	0.005	0.006	0.004	0.006	0.005	0
Fe	0.003	0.003	0.002	0.001	0.005	0.01	0.008	0.005	0
Cu	0.007	0.008	0.005	0.005	0.009	0.015	0.011	0.009	0
Bi	0.88	0.91	0.91	0.90	0.92	0.90	0.90	0.90	0.90
Te	1.00	0.97	0.97	0.98	0.95	0.96	0.97	0.97	0.99

Note: Analyses #1–7 are results of WDS analyses listed in weight %. Composition #8 is mean result of the seven point analyses (WDS). Analysis #9 pertains to results of an SEM/EDS analysis. Other elements (Co, Pt, Sb, Pb, As and S) were sought (WDS), but not detected. The bottom part of the table shows the compositions recalculated on the basis of three atoms per formula unit.

Table 4. Measured and calculated X-ray powder diffraction data (d in Å) for ognitite*.

I_{meas}	I_{calc}	d_{meas}	d_{calc}	$h\ k\ l$	I_{meas}	I_{calc}	d_{meas}	d_{calc}	$h\ k\ l$
10	9	5.39	5.3850	0 0 1	10	3	1.252	1.2506	1 2 1
15	12	3.39	3.4017	1 0 0		8		1.2506	2 1 1
100	**29**	**2.880**	**2.8760**	0 1 1	10	4	1.237	1.2346	2 0 3
	71		2.8760	1 0 1		2		1.2346	0 2 3
10	11	2.697	2.6925	0 0 2	–	3	–	1.1602	1 2 2
30	**13**	**2.110**	**2.1112**	0 1 2	–	3	–	1.1602	2 1 2
	13		2.1112	1 0 2	–	3	–	1.1339	3 0 0
30	**28**	**1.968**	**1.9640**	1 1 0	5	6	1.112	1.1104	1 1 4
–	3	–	1.8451	1 1 1	–	4	–	1.0453	1 2 3
–	2	–	1.7009	2 0 0	–	2	–	1.0453	2 1 3
15	**11**	**1.625**	**1.6219**	0 2 1	–	1	–	1.0450	0 3 2
	5		1.6219	2 0 1	–	1	–	1.0450	3 0 2
20	**10**	**1.589**	**1.5875**	0 1 3	–	1	–	1.0268	0 1 5
	4		1.5875	1 0 3	–	2	–	1.0268	1 0 5
	12		1.5867	1 1 2	–	1	–	0.9293	1 3 1
5	3	1.440	1.4380	0 2 2	–	2	–	0.9099	0 2 5
	3		1.4380	2 0 2					
–	2	–	1.3463	0 0 4					
–	1	–	1.3250	1 1 3					
–	1	–	1.2857	2 1 0					

*Calculated diffraction pattern obtained with the atom coordinates reported in Table 6 (only reflections with $I_{rel} \geq 1$ are listed). The strongest diffraction lines are given in bold.

Table 5. Data and experimental details for the selected ognitite crystal.

Crystal data	
Ideal formula	NiBiTe
Crystal size (mm)	0.040 × 0.050 × 0.060
Form, colour	Block, black
Crystal system, space group	Trigonal, *P*3*m*1
a, c (Å)	3.928(1), 5.385(1)
V (Å^3)	71.95(4)
Z	1
Calculated density (g/cm^3)	8.75
μ (mm^{-1})	77.18
Data collection	
Instrument	Oxford Diffraction Xcalibur 3
Radiation type, wavelength	Mo$K\alpha$ (λ = 0.71073 Å)
Temperature (K)	293(3)
Detector-to-sample distance (cm)	6
Number of frames	348
Measuring time (s)	50
Maximum covered 2θ (°)	74.26
Absorption correction	Multi-scan (Oxford Diffraction, 2006)
Collected reflections	1325
Unique reflections	167
Reflections with $F_o > 4\sigma(F_o)$	81
T_{min}, T_{max}	0.100, 0.112
R_{int}	0.0286
R_σ	0.0347
Range of h, k, l	$-6 \leq h \leq 6$, $-6 \leq k \leq 6$, $-6 \leq l \leq 9$
Refinement	
Refinement	Full-matrix least squares on F^2
Final R_1 [$F_o > 4\sigma(F_o)$]	0.0276
Final R_1 (all data)	0.0460
GoF	0.943
Number refined parameters	11
$\Delta\rho_{min}$, $\Delta\rho_{max}$ (e^- Å^{-3})	−1.01, 1.83

are: $a = 3.928(1)$ Å, $c = 5.385(1)$ Å and $V = 71.95(4)$ Å^3, with $Z = 1$. The c:a ratio calculated from the unit-cell parameters is 1.37.

The powder X-ray diffraction data (Table 4), obtained on the same fragment as used for the single-crystal study, are: $a = 3.9332(4)$ Å, $c = 5.3920(6)$ Å and $V = 72.24(1)$ Å^3.

Crystal structure of ognitite

A small fragment (0.040 mm × 0.050 mm × 0.060 mm) was hand-picked from the ognitite grain (Fig. 4) and examined with an Oxford Diffraction Xcalibur single-crystal diffractometer equipped with an Oxford Diffraction CCD detector, with graphite-monochromatised Mo$K\alpha$ radiation (λ = 0.71073 Å). The collected data were integrated and corrected for standard Lorentz and polarization factors with the *CrysAlis RED* package (Oxford Diffraction, 2006). The program *ABSPACK* in *CrysAlis RED* (Oxford Diffraction, 2006) was used for the absorption correction. Details of the selected crystal, data collection, and refinement are given in Table 5. The calculated value of the R-factor is $R_1 = 0.0276$ for 81 reflections with $F_o > 4\sigma(F_o)$.

Although the statistical tests ($|E^2-1| = 0.756$) suggested an acentric space-group, the crystal structure was initially refined starting from the atomic coordinates of melonite, $NiTe_2$ (Peacock and Thompson, 1946) and using the program *SHELXL-97* (Sheldrick, 2008). Given the observed larger unit-cell volume of ognitite (i.e. 71.95 Å^3) compared to melonite (i.e. 66.93 Å^3; Peacock and Thompson, 1946), the

site-occupancy factor at the crystallographic sites was allowed to vary (Ni *vs.* structural vacancy at the 1*a* site, and Bi *vs.* Te at the 2*d* site) using scattering curves for neutral atoms taken from the *International Tables for Crystallography* (Wilson, 1992). After several cycles of anisotropic refinement, a final R_1 = 0.0795 was achieved, but the atomic displacement parameter at the 2*d* position was abnormally high and asymmetric, thus suggesting a split into two positions. The introduction of two partially occupied (50%) positions (one partially occupied by Bi and one partially occupied by Te) led the R_1 index to 0.0608. At this stage, given the indication coming from the normalised structure-factors, we decided to try to solve the structure in the non-centrosymmetric space-group *P*3*m*1, which allows the separation of the 2*d* position into two positions, 1*b* and 1*c*. The new refinement (R_1 = 0.0276) showed that Bi and Te are completely ordered at 1*b* and 1*c*, respectively, with Bi probably being replaced by 0.03 Ni (according to the refined mean number of electrons at the site). The Te–Ni and Bi–Ni bond distances vary accordingly: the Te–Ni distance (2.575 Å) is identical to that observed in melonite (2.575 Å; Peacock and Thompson, 1946), whereas the Bi–Ni distance (2.696 Å) is in agreement with those observed in parkerite, $Ni_3Bi_2S_2$ (2.64–2.86 Å; Fleet, 1973*b*). Ognitite exhibits a brucite-type structure (Fig. 5). The edge-sharing $NiTe_3Bi_3$ octahedra form sheets parallel to (0001); the sheets are linked by van der Walls interactions.

Atom coordinates, site occupancies, and equivalent isotropic displacement parameters are given in Table 6. Selected bond-distances are given in Table 7. A crystallographic information file has been deposited as supplementary material (see below)

Ognitite is thus related to melonite; however, it differs compositionally (i.e. the marked Bi-enrichment) and structurally, because atoms of Bi and Te are ordered at two specific sites, leading to the loss of the centre of symmetry in the crystal structure, corresponding to a variant of the CdI_2-2*H* structure-type. An additional characterisation of kitkaite (NiTeSe; Häkli *et al.*, 1965) is probably required to check whether it also belongs to that structure-type.

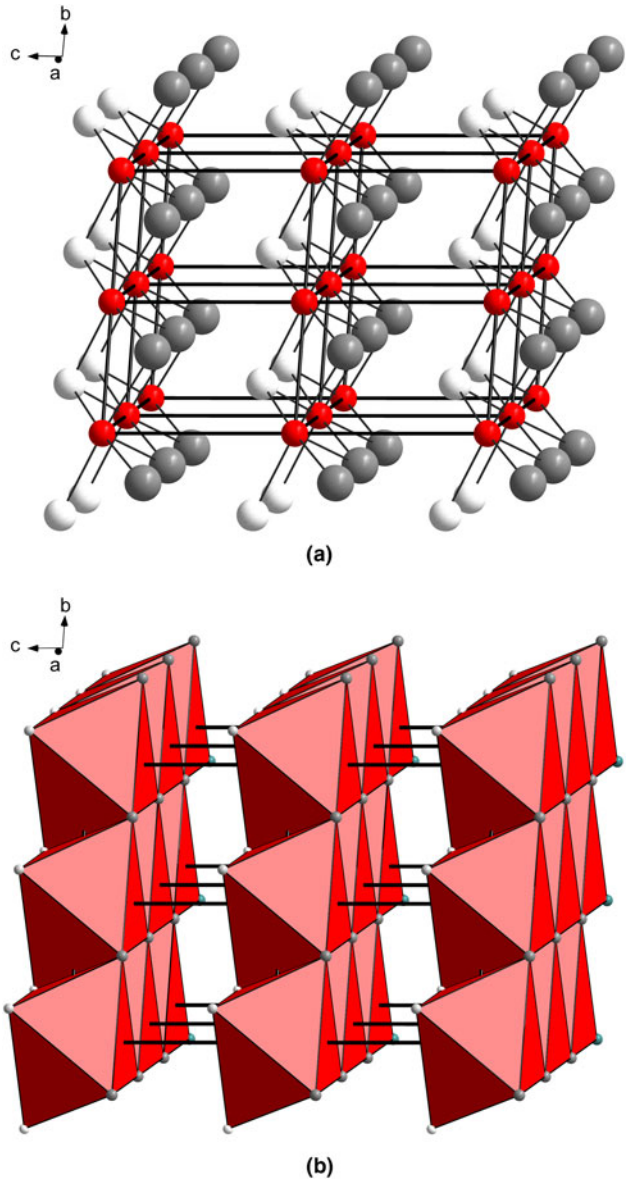

Fig. 5. The crystal structure of ognitite. (*a*) Ball and stick representation: red, white and grey spheres refer to Ni, Te and Bi, respectively; (*b*) polyhedral representation. The unit-cell and the orientation of the figures are outlined.

Co-rich maucherite and zoning in Ni–(Co) arsenides

As noted, the anomalously Co-rich variant of maucherite occurs in the core of a zoned grain (Figs 2*b*, 6*a*,*b*). The rim, composed of orcelite, is essentially devoid of Co (<0.1 wt.%), in contrast to the core zone, which contains ~8 to 10 wt.% Co (or 1.7–2.0 Co apfu: Table 8, #1–6). At least in some cases, the quantitative SEM/EDS method is preferable in analysing narrow zones or tiny phases. Indeed, the SEM/EDS composition (#6, Table 8) is somewhat closer to the ideal stoichiometry; nevertheless, the WDS results obtained (Table 8, #1–5) are consistent.

Our results of the synchrotron micro-Laue diffraction followed by a monochromator energy scan yielded the following cell parameters for the Co-rich maucherite at Ognit: a = 6.85(2) and c = 21.83(5) Å. Thus, these data agree well with those known for the 'normal' phase of maucherite (Co-free; Fleet, 1973*a*).

The orcelite rim corresponds to Ni_5As_2 (Table 8, #7). The structure of orcelite [$Ni_{5-x}As_2$; x = 0.25] represents a distorted variant of the Pd_5Sb_2 structure (Bindi *et al.*, 2014).

As noted, the Co-rich maucherite–orcelite crystal is hosted by a matrix of fine intergrowths of serpentine and clinochlore (Fig. 2). Five grains of serpentine (WDS data) yielded the composition $(Mg_{2.69-2.74}Fe_{0.09-0.11}Al_{0.02-0.08}Cr_{0-0.02}Mn_{<0.01}Ni_{<0.01})_{\Sigma 2.83-2.90}Si_{2.03-2.08}O_5(OH)_4$ (calculated for O = 7 apfu). The Mg# index [100Mg/(Mg + Fe^{2+} + Mn)] is high: ~97.

Compositions of six grains of clinochlore analysed (WDS) in this sample are uniformly rich in Mg, and in Cr, with 2.93–3.21 wt.% Cr_2O_3, and correspond to $(Mg_{4.57-4.70}Fe_{0.21-0.24}Mn_{<0.01}Ni_{\leq 0.01})_{\Sigma 4.80-4.96}Al_{1.0}(Si_{3.00-3.09}Al_{0.73-0.80}Cr_{0.22-0.25}Ti_{\leq 0.01})_{\Sigma 4.01-4.10}O_{10}(OH)_8$ (for O = 14 apfu). Their values of the Mg# index are correspondingly high: up to ~96.

The skeletal grains of chromite associated with the zoned grain of Co-rich maucherite–orcelite (Fig. 2*a*) are weakly Mg-rich, with Mg# in the range 17–22, and are low in aluminium (≤6.5 wt.% Al_2O_3); they display very high values of Cr# [100Cr/(Cr + Al + Fe^{3+}]: 85–92 (Table 1). In addition, elevated levels of Ti (0.7–1.4 wt.% TiO_2), V (≤0.3 wt.% V_2O_3), Mn (0.9–1.0 wt.% MnO), and Zn (0.5–0.7 wt.% ZnO) are present. The chromite grains have a narrow rim of virtually pure magnetite (Fig. 3, Table 1, #10).

Table 6. Atoms, site occupancy factors (s.o.f.), fractional atomic coordinates and anisotropic displacement parameters (Å^2) for the ognitite crystal extracted.

Atom	s.o.f.	*x/a*	*y/b*	*z/c*	U^{11}	U^{22}	U^{33}	U^{23}	U^{13}	U^{12}	U_{eq}
Ni	$Ni_{1.00}$	0	0	−0.0002(19)	0.0267(7)	0.0267(7)	0.031(2)	0	0	0.0134(4)	0.0283(8)
Bi	$Bi_{0.97(2)}Ni_{0.03}$	⅓	⅔	0.72947(2)	0.0436(9)	0.0436(9)	0.063(2)	0	0	0.0218(5)	0.050(1)
Te	$Te_{1.00}$	⅔	⅓	0.2267(4)	0.033(1)	0.033(1)	0.022(1)	0	0	0.0166(6)	0.0295(9)

Table 7. Bond distances (in Å) in the structure of ognitite.

Ni–Te ×3	2.575(5)	Ni–Ni	3.334(2)
Ni–Bi ×3	2.696(5)		
Bi–Te	3.509(3)	Te–Te	3.928(2)
Bi–Bi	3.928(2)		

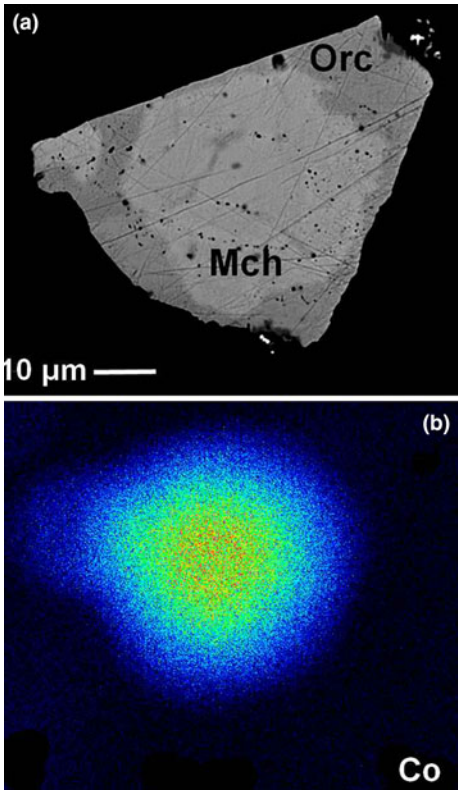

Fig. 6. BSE image (*a*) of the zoned grain of Co-rich maucherite (core: Mch) and orcelite (rim: Orc) hosted by serpentine. (*b*) False-colour X-ray map showing the distribution of Co in the zoned grain of Ni–(Co) arsenides.

Discussion and conclusions

We have described two highly unusual species of Ni ore minerals found in mineralised zones in the Ognit ultramafic complex, Eastern Sayans, Russia. The anomalously high level of Bi in ognitite [$Ni_{1.1}Bi_{0.9}Te$] evidently cannot be explained by incorporation of the merenskyite and moncheite components in solid solution (Table 3). There is no evidence that the proximity to granodiorite (Fig. 1*b*) is an important factor, as there is no evidence of assimilation of xenoliths. And efforts to synthesise the phase NiBiTe in long-duration experiments at 200°, 400° and 600°C were not successful; the bismuth present in the charge crystallised to Bi + Bi_2Te (Barkov *et al.*, 2017*a*). Thus, we suggest that special conditions were important to stabilise the markedly Bi-enriched ognitite structure instead of that of common melonite.

Table 8. Compositions of Co-rich maucherite and associated orcelite in a zoned grain from the Ognit complex.

#	1	2	3	4	5	6	7
Wt.%							
Ni	45.4	45.42	45.77	45.58	46.54	44.82	65.98
Co	9.56	9.59	9.55	8.71	8.63	8.43	–
Fe	0.55	0.58	0.57	0.7	0.75	0.57	0.68
As	44.76	44.49	44.1	44.47	44.5	46.95	33.85
S	0.53	0.53	0.52	0.49	0.5	0.48	–
Te	0.07	0.03	0.03	–	0.03	–	–
Sb	0.04	–	0.13	0.05	0.02	–	–
Total	100.91	100.64	100.68	100	100.97	101.25	100.51
Atoms per formula unit							
Ni	9.42	9.44	9.51	9.54	9.64	9.31	4.98
Co	1.98	1.98	1.98	1.82	1.78	1.74	–
Fe	0.12	0.13	0.12	0.15	0.16	0.12	0.05
As	7.27	7.24	7.18	7.3	7.22	7.64	2
S	0.2	0.2	0.2	0.19	0.19	0.18	–
Te	0.006	0.003	0.003	–	0.003	–	–
Sb	0.004	–	0.013	0.005	0.002	–	–
Ni + Co + Fe	11.51	11.55	11.61	11.51	11.58	11.18	5.03
As + S	7.48	7.45	7.38	7.48	7.41	7.82	2

Note: Results of WDS (#1–5) and SEM/EDS (#6, 7) analyses are listed in the top part of the table in wt.%. Analyses #1–6 pertain to maucherite. Analysis #7 pertains to orcelite. Atomic proportions, are based on a total of 19 atoms per formula unit (apfu) for maucherite, and on two apfu S for orcelite.
'–' = not detected.

The uniqueness of the Co-rich variant of maucherite also implies the existence of strongly atypical conditions. The high values of Mg# (95–97) of serpentine and clinochlore reflect the highly Mg-rich compositions of primary grains of olivine and pyroxene crystallised in the primitive ultramafic cumulates. We propose that the skeletal texture of the associated grains of chromite (Fig. 2a) indicates difficulties in their nucleation. They could well provide an indication of rapid cooling in the system, possibly related to the degassing of the magma at an advanced stage of crystallisation of the complex, reflected in the prominent metasomatic aureole at the contact (Fig. 1*b*). Effects of supercooling and metastable crystallisation were observed in the Pados-Tundra ultramafic complex, Kola Peninsula, Russia (Barkov *et al.*, 2016, 2017*b*), for example.

We thus suggest a mechanism of metastable crystallisation to explain the anomalous compounds at Ognit. An elevated fluid pressure could have existed in the ore-forming system. The anomalously Bi-rich composition of ognitite could well represent a late-crystallising phase formed in a fluid-saturated environment from a droplet of residual melt enriched in Ni, Bi and Te. These elements are incompatible in the host chalcopyrite, as are Ag and Pb, present in the coexisting hessite and altaite. The shared boundary with native Bi (Fig. 4) is consistent with various occurrences of native elements and alloys (i.e. native silver, Ag–Au alloy, auricupride, awaruite, native copper and graphite), which indicate the existence at Ognit of reducing conditions (Shvedov and Barkov, 2017).

These conditions point to a probable stability-field at Ognit of the reduced form, As^{3+}, rather than As^{5+}, which seems to be typical of mantle-related serpentinites (Hattori *et al.*, 2005). The Ni-rich arsenides, including their grains with their original shapes, are quite common accessory phases in the ore zones at Ognit; these formed from droplets of As-rich melts (Shvedov and Barkov, 2017). The documented occurrences of Ni arsenides thus reflect arsenide saturation of the sulfide liquid (cf., Piña *et al.*, 2014); an initial content of ≥0.1 wt.% As is considered sufficient to ensure saturation in an arsenide (Fleet *et al.*, 1993). The zonation is documented in the grain composed of the Co-rich maucherite in the core and Co-depleted orcelite in the rim (Figs 2*b*; 6*a*,*b*). In other layered complexes, zoned grains of Ni–Co–(PGE) sulfarsenides are developed instead (e.g. Barkov *et al.*, 1999).

If the equilibrium crystallisation is postulated at Ognit, results of experimental studies are then applicable. The melting point of synthetic Ni_5As_2 (orcelite equivalent) is 998°C; the upper thermal stability limit of $Ni_{11}As_8$ (maucherite) is 830°C (Yund, 1961; Singleton and Nash, 1987). These values suggest that orcelite is expected to crystallise before maucherite if they coexist under normal conditions. In contrast, we observe that the Co-enriched maucherite occurs in the core; thus, it presumably nucleated first and before the orcelite phase developed in the rim. If so, we can reasonably propose that the incorporation of Co increases, to a notable extent, the melting point of $Ni_{11}As_8$, in contrast to the effect observed from the incorporated Pd (cf., Gervilla *et al.*, 1994). This possibility requires an experimental confirmation, however. The Co analogue of maucherite does not seem to have been reported, and thus was probably not obtained by synthesis. However, synthetic Co_5As_2 (space group $P6_3cm$; i.e. prototype of Pd_5Sb_2), related to orcelite, exists in the system Co–As, in which it is a high-temperature phase; it undergoes a disproportionation transformation to (α-Co) + β-Co_2As at 867°C (Ishida and Nishizawa, 1990, and references therein). Note that the orcelite phase is essentially devoid of Co in the rim, in spite of the existence of the cobalt analogue of orcelite. This feature also implies that Co was preferentially incorporated into maucherite as the early phase, a reflection of the relatively high temperature of its crystallisation.

Supplementary material. To view supplementary material for this article, please visit https://doi.org/10.1180/mgm.2019.31

Acknowledgements. We are grateful to an anonymous referee, Drs. Peter Leverett, Anna Vymazalová, Irina Galuskina, Roger Mitchell, and to the editorial staff for their valuable comments. This research required access to beamline 12.3.2 at the Advanced Light Source, which is a DOE Office of Science User Facility under contract #DE-AC02-05CH11231. A.Y.B. gratefully acknowledges a partial support of this investigation by the Russian Foundation for Basic Research (projects #RFBR 16-05-00884 and # RFBR 19-05-00181). C.J.S. acknowledges Natural Environment Research Council grant NE/M010848/1 "Tellurium and Selenium Cycling and Supply".

References

Barkov A.Y., Thibault Y., Laajoki K.V.O, Melezhik V.A. and Nilsson L.P. (1999) Zoning and substitutions in Co–Ni–(Fe)–PGE sulfarsenides from the Mount General'skaya layered intrusion, Arctic Russia. *The Canadian Mineralogist*, **37**, 127–142.

Barkov A.Y., Nikiforov A.A., Halkoaho T.A.A. and Konnunaho J.P. (2016) The origin of spheroidal patterns of weathering in the Pados-Tundra mafic-ultramafic complex, Kola Peninsula, Russia. *Bulletin of the Geological Society of Finland*, **88**, 105–113.

Barkov A.Y., Shvedov G.I., Flemming R.L., Vymazalová A. and Martin R.F. (2017*a*) Melonite from Kingash and Kuskanak, Eastern Sayans, Russia, and the extent of Bi-for-Te substitution in melonite and synthetic Ni(Te, Bi)$_{2-x}$. *Mineralogical Magazine*, **81**, 695–705.

Barkov A.Y., Nikiforov A.A. and Martin R.F. (2017*b*) The structure and cryptic layering of the Pados-Tundra ultramafic complex, Serpentinite belt, Kola Peninsula, Russia. *Bulletin of the Geological Society of Finland*, **89**, 35–56.

Barkov A.Y., Bindi L., Winkler B., Morgenroth W., Shvedov G.I., Martin R.F., Zaccarini F., Stan C.V., Tamura N. and Stanley C.J. (2019) Ognitite, IMA 2018-006a. CNMNC Newsletter No. 47, February 2019, page 146; *Mineralogical Magazine*, **83**, 143–147.

Barnes S.J. and Roeder P. (2001) The range of spinel compositions in terrestrial mafic and ultramafic rocks. *Journal of Petrology*, **42**, 2279–2302.

Bindi L., Tredoux M., Zaccarini F., Miller D.E. and Garuti G. (2014) Non stoichiometric nickel arsenides in nature: the structure of orcelite, $Ni_{5-x}As_2$ (x = 0.25), from the Bon Accord oxide body, South Africa. *Journal of Alloys and Compounds*, **601**, 175–178.

Cabri L.J. and Laflamme J.H.G. (1976) The mineralogy of the platinum-group elements from some copper-nickel deposits of the Sudbury area, Ontario. *Economic Geology*, **71**, 1159–1195.

Ernst R.E., Hamilton M.A. and Soderlung U. (2012) A *proposed 725 Ma Dovyren–Kingash LIP of southern Siberia, and possible reconstruction link with 725–715 Ma Franklin LIP of North Laurentia*. Abstract Volume, 35, GAC-MAC Joint Annual Meeting "Geoscience at the Edge" (May 27–29, 2012, St. Johns, Newfoundland and Labrador, Canada).

Fleet M.E. (1973*a*) The crystal structure of maucherite ($Ni_{11}As_8$). *American Mineralogist*, **58**, 203–210.

Fleet M.E. (1973*b*) The crystal structure of parkerite ($Ni_3Bi_2S_2$). *American Mineralogist*, **58**, 435–439.

Fleet M.E., Chryssoulis S.L., Stone E.S. and Weisener C.G. (1993) Partitioning of platinum-group elements and Au in the Fe–Ni–Cu–S system: Experiments on the fractional crystallization of sulfide melt. *Contributions to Mineralogy and Petrology*, **115**, 36–44.

Garuti G. and Rinaldi R. (1986) Mineralogy of melonite-group and other tellurides from the Ivrea–Verbano basic complex, western Italian Alps. *Economic Geology*, **81**, 1213–1217.

Gervilla F., Makovicky E., Makovicky M. and Rose-Hansen J. (1994) The system Pd–Ni–As at 790° and 450°C. *Economic Geology*, **89**, 1630–1639.

Gervilla F., Cabri L.J., Kojonen K., Sie S.H., Papunen H. and Hach-Alí F.P. (2000) Trace platinum group elements in arsenides and sulfarsenides from magmatic ores: An electron microprobe and proton microprobe (micro-PIXE technique) study. *Cadernos Lab. Xeoloxico de Laxe Coruna*, **25**, 103–105.

Gladkochub D.P., Wingate M.T.D., Pisarevsky S.A., Donskaya T.V., Mazukabzov A.M., Ponomarchuk V.A. and Stanevich A.M. (2006) Mafic intrusions in southwestern Siberia and implications for a Neoproterozoic connection with Laurentia. *Precambrian Research*, **147**, 260–278.

Gritsenko Yu.D. and Spiridonov E.M. (2008) Maucherite from metamorphic-hydrothermal assemblages of the Noril'sk ore field. *Geology of Ore Deposits*, **50**, 590–598.

Häkli T.A., Vuorelainen Y. and Sahama T.G. (1965) Kitkaite (NiTeSe), a new mineral from Kuusamo, northeast Finland. *American Mineralogist*, **50**, 581–586.

Hattori K., Takahashi Y., Guillot S. and Johanson Bo (2005) Occurrence of arsenic (V) in forearc mantle serpentinites based on X-ray absorption spectroscopy study. *Geochimica et Cosmochimica Acta*, **69**, 5585–5596.

Ishida K. and Nishlzawa T. (1990) The As–Co (arsenic–cobalt) system. *Bulletin of Alloy Phase Diagrams*, **11**, 550–554.

Makovicky M., Makovicky E., and Rose-Hansen J. (1992) The phase system Fe–Pt–As–S at 850°C and 470°C. *Neues Jahrbuch für Mineralogie*, **10**, 441–453.

Makovicky E. and Merlino S. (2009) OD (order–disorder) character of the crystal structure of maucherite Ni_8As_{11}. *European Journal of Mineralogy*, **21**, 855–862.

Mekhonoshin A.S., Tolstykh N.D., Podlipsky M.Yu., Kolotilina T.B., Vishnevsky A.V. and Benedyuk Yu.P. (2013) PGE mineralization of dunite–wehrlite massifs at the Gutara-Uda interfluve, Eastern Sayan. *Geology of Ore Deposits* **55**, 162–175.

Mekhonoshin A.S., Kolotilina T.B. and Doroshkov A.A. (2018) Geochemical model for the formation of the Medek platinum-bearing dunite-wehrlite intrusion (East Sayan, Russia). *Russian Geology and Geophysics*, **59**, 1603–1615.

Oxford Diffraction (2006) *CrysAlis RED (Version 1.171.31.2) and ABSPACK in CrysAlis RED*. Oxford Diffraction Ltd, Abingdon, Oxfordshire, England.

Özkurt B. (2012) Effects of Ni substitution in Bi-2212 superconductors. *Journal of Superconductivity and Novel Magnetism*, **25**, 1775–1779.

Peacock M.A. and Thompson R.M. (1946) On melonite from Quebec and the crystal structure of $NiTe_2$. *American Mineralogist*, **31**, 204.

Petruk W., Harris D.C. and Stewart J.M. (1971) Characteristics of the arsenides, sulpharsenides and antimonides. *The Canadian Mineralogist*, **11**, 150–186.

Piña R., Gervilla F., Barnes S.-J. and Lunar O.R. (2014) Liquid immiscibility between arsenide and sulfide melts: evidence from a LA–ICP–MS study in magmatic deposits at Serranía de Ronda (Spain). *Mineralium Deposita*, **50**, 265–279.

Prichard H.M., Fisher P.C., McDonald I., Knight R.D., Sharp D.R. and Williams J.P. (2013) The distribution of PGE and the role of arsenic as a collector of PGE in the Spotted Quoll nickel ore deposit in the Forrestania Greenstone Belt, Western Australia. *Economic Geology*, **108**, 1903–1921.

Raič S., Mogessie A., Benkó Z., Molnár F., Hauck S. and Severson M. (2015) Arsenic-rich Cu-Ni-PGE mineralization in Wetlegs, Duluth complex, St. Louis county, Minnesota, USA. *The Canadian Mineralogist*, **53**, 105–132.

Sheldrick G.M. (2008) A short history of SHELX. *Acta Crystallographica*, **A64**, 112–122.

Shvedov G.I. and Barkov A.Y. (2017) Primary and alteration assemblages of platinum-group minerals from the Ognit complex, Irkutskaya oblast, Eastern Sayans, Russia. *Neues Jahrbuch für Mineralogie Abhandlungen: Journal of Mineralogy and Geochemistry*, **194**, 35–48.

Singleton M. and Nash P. (1987) The As–Ni (arsenic–nickel) system. *Journal of Phase Equilibria*, **8**, 419–422.

Tamura N. (2014) XMAS: A Versatile Tool for Analyzing Synchrotron X-ray Microdiffraction Data. Pp. 125–155 in: *Strain and Dislocation Gradients from Diffraction* (R. Barabash and G. Ice, editor). Imperial College Press, London, UK.

Tolstykh N.D., Polyakova G.V., Izokh A.E., Podlipsky M.Yu., Mekhonoshin A.S., Orsoev D.A. and Kolotilina T.B. (2014) *Cu–Ni–PGE deposits of east Siberia hosted by Neoproterozoic mafic-ultramafic complexes*. Pp. 138–140 in: Abstract Volume 2014 Convention 11th International Conference on Gondwana to Asia 20–21 September, Beijing, China IAGR Conference Series No. 20.

Wagner T. and Lorenz J. (2002) Mineralogy of complex Co–Ni–Bi vein mineralization, Bieber deposit, Spessart, Germany. *Mineralogical Magazine*, **66**, 385–407.

Wilson A.J.C., Ed. (1992) *International Tables for Crystallography, Volume C: Mathematical, Physical and Chemical Tables*. Kluwer Academic, Dordrecht, NL.

Yilmaz F., Kilicaslan M.F., Atanur O.M., Hong S.-J. and Uzun O. (2012) Effects of substitution of Al and Bi for Ni on structure and hydrogen storage properties of $LaNi_{4.7-x}Al_{0.3}Bi_x$ ($x = 0.1$, 0.2, 0.3) alloy. *Japanese Journal of Applied Physics*, **51**, 09MB01.

Yund R.A. (1961) Phase relations in the system Ni–As. *Economic Geology*, **56**, 1273–1296.